water

MDPI

Article

Bedload Velocity and Backscattering Strength from Mobile Sediment Bed: A Laboratory Investigation Comparing Bistatic Versus Monostatic Acoustic Configuration

Slaven Conevski [1,*], Rui Aleixo [2], Massimo Guerrero [3] and Nils Ruther [1]

1 Department of Civil and Environmental Engineering, Norwegian Institute of Science and Technology, 7491 Trondheim, Norway; nils.ruther@ntnu.no
2 CERIS—Civil Engineering Research and Innovation for Sustainability, Av. Rovisco Pais, 1049-003 Lisboa, Portugal; rui.aleixo@tecnico.ulisboa.pt
3 Department of Civil, Chemical, Environmental, and Materials Engineering, University of Bologna, 40131 Bologna, Italy; massimo.guerrero@unibo.it
* Correspondence: slaven.conevski@ntnu.no; Tel.: +479-060-3332

Received: 30 October 2020; Accepted: 20 November 2020; Published: 26 November 2020

Abstract: Despite the many advantages of using active ultrasound sonars, recent studies have shown that the specific acoustic geometry, signal-processing configuration, and complex surface-volume scattering process at the riverbed introduce several uncertainties in bedload estimation. This study presents a comparison of bedload velocity and bottom echo intensity measurements performed by monostatic and bistatic active ultrasound systems. The monostatic configuration is widely applied in the field to measure the apparent velocity at the riverbed with an acoustic current Doppler profiler (ADCP). Two laboratory investigations were conducted in two different hydraulic facilities deploying ADCP Stream Pro, monostatic and bistatic acoustic velocity profilers, manufactured by Ubertone. The bistatic instruments provided more accurate bedload velocity measurements and helped in understanding the acoustic sampling of the monastic systems. The bistatic profiles succeeded in measuring a profile over the active bedload layer, and the monostatic instruments resulted in different bedload velocity estimations depending on the acoustic resolution and sampling. The echo intensity increased in the cells measured within the active bedload layer with respect to the cell measuring the water column above. The cells that sampled the immobile bed surface beneath the bedload layer showed a reduction of the echo intensity compared with the cells above. The acoustic sampling, which combines the measurement volume geometry and internal processing, seems crucial for more accurate outputs. Future research about the use of monostatic instruments in the field should aim to define the best possible setting for the acoustic parameters at a given bedload condition that may be tuned by evaluating the backscattering at the river bottom together with the apparent bedload velocity.

Keywords: bedload; sediment transport; ultrasound measurements; hydroacoustics; surface and volume backscattering

1. Introduction

Sediments transported by rolling, sliding, or saltating on the bottom of an aquatic environment are called bedload. The topmost stratum of the streambed, which is partially mobile, is called the active bedload layer [1]. Quantifying the mass of bedload that moves within the active layer per unit time defines the bedload transport rate.

Accurate estimation of bedload transport characteristics in a riverine environment is still an open problem in engineering. Measuring the transport rate and using direct conventional methods (i.e., bedload traps or samplers) is notoriously difficult and labor-intensive [2]. Therefore, bedload measurements are seldom available and sometimes considered statistically unreliable. The uncertainty associated with conventional techniques can be characterized as systematic and stochastic [3,4]. The sources of the systematic uncertainty result from the technical design of the sampler, such as disturbance of the riverbed, correct positioning, length of the sampling time, and clogging of the mesh [5]. The stochastic uncertainty originates from the sporadic and rather inhomogeneous nature of the motion of bedload particles [4,6].

To overcome these problems, new surrogate methods have recently been introduced, allowing nonintrusive, continuous, and more accurate measurements. These surrogate techniques involve videography, active and passive acoustic sensing, seismic registering mechanisms, and so forth.

In the last few decades, various videography techniques have been developed to investigate the behavior of bedload particles, mostly on a small scale and in controlled conditions, involving analyzing individual particle tracks and velocities [6–9], denoted as particle tracking velocimetry (PTV). Additional image processing techniques, such as optical flow and image differencing, have been successfully applied to calculate mobile bed velocity, the surface concentration of mobile particles, and even the shape of particles in reasonably set-up conditions [10–14]. However, image processing techniques are limited to laboratory applications due to light conditions, small sampling areas, large data storage requirements, and relatively difficult installation.

Hydroacoustic techniques are easy to deploy, do not require extensive data storage, and offer continuous measurements even in high-flow situations. Acoustic sensors are typically divided into two categories: active and passive. Passive sensor-based techniques record the acoustic noise of the bedload particle collisions, whereas active sensor-based systems register the effect of the motion of the particles on the reflected acoustic signal from the riverbed. Passive acoustic systems consist of a set of hydrophones and geophones that are relatively easy to install. Data postprocessing can effectively distinguish the noise generated by bedload particles; however, its calibration can be exhaustive and unreliable [15,16].

Active acoustic systems can be monostatic, equipped with a transducer that emits and receives the acoustic signal and bistatic when the transmitter and receivers are reasonably separated. Acoustic current Doppler profilers (ADCPs) are the most popular active acoustic system and frequently used for measuring river discharge and flow velocity in conditions with a changing water depth across a river channel. ADCPs' diverging beam configuration enables taking measurements at variable water depths. Given this advantage, ADCPs were also applied for bathymetric surveying and measuring bedload velocity. Regarding bedload measurements, Rennie [17] initially reported that the velocity measured by the bottom tracking (BT) feature of an ADCP is well correlated to the bedload transport rate. This technique introduced the BT velocity bias, defined as the difference between the GPS boat velocity and boat velocity measured by the BT feature of the ADCP ($v_a = v_{gps} - v_{BT}$). This velocity is also denoted as the apparent bedload velocity (v_a) [14,17]. Studies have reported a good correlation between apparent bedload velocity and bedload transport [18], attempting to develop site-specific or grain-size-dependent relationships with the bedload transport rate [19]. In addition, v_a was successfully used for mapping bedload transport intensity [20] and evaluating morphodynamical processes in large rivers [21]. An analytical relationship between the real bedload particle velocity and apparent bedload velocity, considering the scattering properties of the mobile and immobile bedload particles, was proposed by Gaeuman and Jacobson [22]. This correlation with the real bedload velocity was experimentally proven using the image processing technique as a comparison [14]. The same study described the coupling problem in the bedload reflected acoustic signal associated with the simultaneous volume scattering of mobile particles and surface scattering of immobile particles beneath. It was noted that different ADCPs do not deliver the same apparent velocity despite measuring the same condition [14,23–26]. The main sources of these differences are due to instrument-specific configurations and signal processing [25], instrument-carrying frequency [14], attenuation occurring in the active

bedload layer [14,26], and reverberation from the surface scattering of immobile bedload particles. All these factors, together with the sporadic nature of the bedload transport, influence acoustic sampling, resulting in erroneous apparent bedload velocity measurements. Part of these errors are efficiently filtered using the water velocity direction [14,25], but some remain nested; thus, each instrument requires specific postprocessing and eventual calibration for the accurate measurement of bedload characteristics [26]. It was recently shown that backscattering strength registered by ADCPs at the same time as the apparent bedload velocity is strongly correlated with the bedload concentration and particle size distribution of the sediments [26]. However, it remains unknown to which degree these sources influence the erroneous velocity and backscatter outcome of the ADCPs; therefore, it is impossible to accurately predict the bedload transport rate.

Bistatic sonar systems are currently still limited to laboratory conditions because of the fixed-range distance, which can be a maximum of 40 to 50 cm and depends on the distance between applied transducers [27]. Bistatic systems, often referred to as acoustic Doppler velocity profilers (ADVP), can deliver detailed velocity profiles close to the bed and estimate the concentration of the material resuspended above the bed [28]. Another laboratory study demonstrated that ADVPs could depict several cells of bedload velocities inside the active layer [13]. Consequently, bistatic acoustic systems allow detailed measurements of bedload transport characteristics, clearly distinguishing between the volume scattering of mobile particles and the surface scattering of the immobile sediment bed. On the contrary, the distinction between volume and surface scattering is one of the key issues with monostatic systems.

This study aims to evaluate and investigate the limitations of monostatic acoustic systems in measuring bedload characteristics compared with bistatic systems to eventually improve the use of ADCP monostatic systems in the field. Two experiments were conducted in the hydraulic laboratories of the Norwegian University of Science and Technology (NTNU) and the University of Bologna (UniBo) with fine (NTNU) and medium-sized sand (UniBo) used as a sediment bed. ADCP Stream Pro (2 MHz) by RDI [29] and Ubertone's ultrasound velocity profilers (UVPs) [30] working on three different frequencies (3 MHz, 1.5 MHz, and 0.5 MHz) were deployed as monostatic instruments. Ubertone's ADVP [27] was used as a bistatic device. It is worth noting that UVPs were used to simulate one beam of the ADCPs, with the advantage of changing some of the instrument parameters. The instruments were tested in different bedload transport conditions, and the bedload mean transport rate was measured by a bedload trap placed at the end of the flume. Simultaneously, high-speed cameras were installed to record the bed sediments, providing an estimation of both the bedload surface concentration and velocity.

The sampling area of the monostatic systems is analyzed in detail as the acoustic sampling limitation induced by the specific beam geometry of the monostatic systems is typically associated with the blanking zone of the ADCPs.

The constraints and ranges of measurement for both systems are analyzed and discussed, specifically focusing on the different velocity ranges measured by the monostatic instruments and the bedload velocity profiles obtained by the bistatic ADVP. The sensitivity of the backscattering strength towards different bedload concentrations is also tested. Finally, this study demonstrates that some limitations of the monostatic system could be resolved by adjusting the acoustic parameters or instrument geometry. The influence of the acoustic beam geometry parameters (e.g., grazing angle, beam opening) on the backscattering strength and Doppler velocity estimation are discussed.

2. Methodology

2.1. Experimental Set-Ups

2.1.1. NTNU Flume: Monostatic Acoustic System

A set of experiments involving monostatic acoustic systems (UVPs and ADCPs) were conducted at the Hydraulic Laboratory of NTNU, Trondheim. The flume was 12.5 m long in total, and the mobile bed section was 10 m long and 0.6 m wide (Figure 1a).

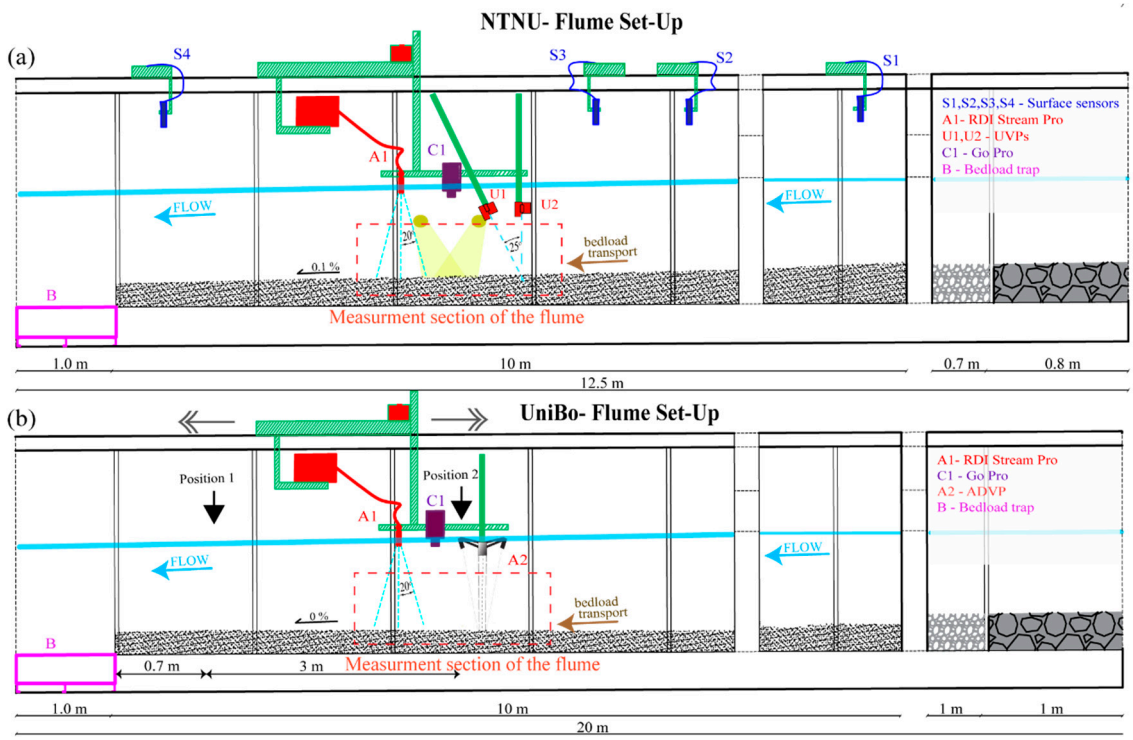

Figure 1. Experimental set-up. (**a**) Norwegian University of Science and Technology (NTNU—ultrasound velocity profiler (UVP)/acoustic current Doppler profiler (ADCP), medium sand, set-up; (**b**) UniBo ADVP/ADCP set-up, coarse sand.

The UVPs were controlled and adjusted using Ubertone's UB-LabX8 data acquisition toolbox [30]. Six probes (transducers) were connected to the UB-LAbX8 processing box. Three different frequencies (3 MHz, 1.5 MHz, and 0.5 MHz) and six transducers were utilized. Three were tilted, forming a 65° grazing angle with the sediment bed, and three were mounted vertically at 90° (Figure 1a). The same set-up was used to collect the data with the ADCP Stream Pro (SPro) system but not at the same time due to a significant increase in the noise level of the UVPs. The SPro data were adopted from Conevski et al. [26]. To avoid interference, UB-Lab used a multiplexing system emitting and receiving pulses for each transducer in a sequence at a given pulse repetition frequency (PRF). The UVPs were used in the experiments sandEXP1 and sandEXP2, whereas the SPro data were only available for sandEXP1 and sandEXP22.

Water level was measured utilizing six acoustic sensors mounted on the top of the flume, and the water velocity was measured with two Nortek ADVs measuring close to the bed and close to the water surface, as shown in Figure 1a.

One high-speed camera (GoPro HERO 6) was mounted above the sampling zone of the UVPs. This camera provided a planar view of the UVP sampling zone and recorded during the entire experiment. The GoPro camera recorded footage at 60 frames per second with 4K resolution at a 30 cm distance from the sediment bed. This resulted in 2–3 pixels per median grain size of the sand and approximately five times the higher range of measurement than the expected bedload particle velocities. The expected sand velocities were estimated using empirical equations [6,8,9,31–33] and varied between 0.05 and 0.2 m s^{-1} for all the experiments.

Medium to fine sand (D_{50} = 0.35 mm) was used as sediment material covering 10 m of the flume's length. The nominal sediment layer thickness ranged within 10–12 cm: 12 cm at the entrance and 10 cm before the bedload trap.

The sediment transport rate was measured employing a bedload trap placed at the end of the flume. The bedload trap was an aluminum box with dimensions 1 m × 1 m × 0.15 m. The load cells

installed underneath the box continuously weighed the collected sediments at a frequency of 50 Hz. Data were averaged and processed according to Conevski et al. [26].

The different transport conditions were reached by changing the flow rate from 80 L/s to 120 L/s, keeping a constant slope of the flume bed of 0.1%. The objective was to obtain the motion of the sand particles without bedforms (sandEXP1) and with bedforms (sandEXP2 and sandEXP21). The difference between the shear velocity (u^*) and critical shear velocity (u_{cr}^*), as reported in Table 1, shows the planned variety of bedload transport conditions. The hydraulic parameters in Table 1 were calculated according to Conevski et al. [14]. The experiments were repeated several times to improve the reliability of the data.

Table 1. Hydraulic parameters.

	EXP	Q	H	U	D_{50}	R_{ep}	u_{cr}^*	u^*
		L/s	m	m s^{-1}	mm	\	m s^{-1}	m s^{-1}
NTNU	sandEXP1	80.00	0.40	0.3	0.35	20.00	0.014	0.015
	sandEXP2	100.00	0.40	0.39	0.35	20.00	0.014	0.019
	sandEXP22	120.00	0.40	0.43	0.35	20.00	0.014	0.021
UniBo	EXP1 POS1	111.68	0.31	0.45	1.00	97.00	0.021	0.023
	EXP1 POS2	111.48	0.31	0.41	1.00	97.00	0.021	0.025
	EXP2 POS1	111.26	0.27	0.58	1.00	97.00	0.021	0.034
	EXP2 POS2	110.97	0.27	0.59	1.00	97.00	0.021	0.038

2.1.2. UniBo Flume: Bistatic Acoustic System

The experiments at UniBo were performed at a 20 m long flume with a loose bed made of medium to coarse sand (D_{50} = 1 mm), equally distributed over a 10 m long reach, as depicted in Figure 1b, with a slope of 0%. The different flow conditions were obtained by changing the water level (Table 1). Low sediment flux and fair deformation of the bed were observed for the first hydraulic condition (EXP1 in Table 1), whereas the second condition resulted in well-defined sediment flux and well-defined dunes (EXP2 in Table 1). Continuous measurements were made with two instruments, the ADVP and ADCP SPro, mounted on a rigid movable frame. In this frame, the two instruments were placed 1 m apart (streamwise direction) and shifted 0.2 m relative to the centerline. The two devices were paired in a sequence that included 5 min of recording the ADCP for each ADVP measurement block for 3 min at a frequency of 5 to 7 Hz. The same test was repeated three times by pairing consequent recordings at two different sections along the channel. This procedure avoided interferences between acoustic pulses from ADVP and ADCP and enabled the measuring at different positions and times along the flume. Two measurement sections of the sediment bed were used to register the data, distanced 0.7 m and 3.65 m from the bedload trap (Figure 1). The experiments were performed five times to eventually account for the influence of the spatial and temporal variability of the bedload motion and the repeatability of the experimental procedure.

Since the experimental set-up and flow conditions were the same as described by Conevski et al. [14], the latter imaging data, acquired with a GoPro HERO 4 working at 4k resolution with 30 frames per second, was used to evaluate the average bedload surface concentration and the bedload surface velocity [12,14].

Finally, as in the NTNU experiment, the mean bedload transport rate was measured at the end of the flume by employing a bedload trap.

2.2. Acoustic Theory

2.2.1. Basic Principles

A transducer of an active sonar emits a burst of acoustic wavelengths (λ) into the water column forming an acoustic pulse (*Pl*). This ultrasonic pulse consists of several wave periods within the bandwidth of the selected transducer. When the pulse is emitted and travels in the water column, it is scattered by the particles present in the water and reflected by the sediment bed. The echo intensity, or the returned signal, contains information correlated with the concentration, shape, and size of the particles [34,35]. The returned signal also contains a shift of the frequency due to the motion of the particles, known as the Doppler shift [30,36]. The Doppler shift is therefore correlated to the particle velocity and used to estimate the real velocity of the particles in the beam direction [37]. To determine the velocity in the flume direction, the transducer must be tilted for an angle to the vertical (20–30°, Table 2), which is typically chosen to be close to the critical angle of reflection [38]. The ultrasound sonars typically use the gate-profiling method to estimate the velocity and the echo intensity at different distances from the transducer. These gates or cells are defined as a slice of the beam with a certain thickness (i.e., cell size) and typically depend on the pulse length, which determines the resolution of measurements.

Table 2. Acoustic parameter.

Type	f	D_t	λ	φ	Near Field	θ	D_s	*PRF*	v_{max}/R_{max}	*PL*	Cell Size
	MHz	**mm**	**mm**	°	**m**	°	**mm**		**m s^{-1}/m**	**mm**	**mm**
UVP	3.0	7.0	0.5	2.0	24.8	25	39	1200	0.30/0.29	4	4.4
UVP	1.5	20.0	1.0	1.4	101.4	25	44	1000	0.49/0.35	4	4.4
UVP	0.5	15.0	3.0	5.7	19.0	25	104	900	1.33/0.38	10.4	10.4
UVP	3.0	7.0	0.5	2.0	24.8	90	7	1200	0.30/0.29	4	4.4
UVP	1.5	20.0	1.0	1.4	101.4	90	20	1000	0.49/0.35	4	4.4
UVP	0.5	15.0	3.0	5.7	19.0	90	15	900	1.33/0.38	10.4	10.4
ADVP	1.0	25.0	1.5	0.0	/	*n.a.*	25	500	1/0.4	1.4	1.4
ADCP SPro	2.0	15.0	0.7	1.3	76.0	20	36	/	2/5	0.7	/

The measured Doppler velocities are typically very noisy; thus, an accurate velocity profile is obtained by internally averaging data from many pulses. The repetition of the ultrasound pulse (*Pl*) gives an accurate velocity estimation, but the sampling itself induces a limitation of the velocity range (Nyquist frequency), which combines with the measurable maximum depth for the needed travel time [37]. Thus, the pulse repetition frequency (*PRF*) determines the measurement maximum ranges of the velocity and depth [30]. However, advanced signal-processing techniques relax some of these limitations [25,26]. The Ubertone instruments rely on the pulse coherent (PC) signal-processing technique, which makes the system dependent on the *Pl* and *PRF* [39] and therefore have lower measurement ranges (Table 2). The RDIs SPro uses a broadband (BB) signal-processing technique that emits two or several pulses in a burst, which shortens the time between the pulse pairs and increases the maximum unambiguous velocity [25,37]. Unfortunately, the details of the signal-processing techniques are not available to the users, and the eventual outperformance into the bedload measurements cannot be fully explored.

2.2.2. Monostatic Sonars

The monostatic sonars have one transducer that receives and emits the acoustic pulse. Each transducer has characteristics that mainly depend on the carrying frequency (f) and diameter of the transducer (D_t). Once the pulse is emitted, it forms an acoustic beam with a cylindrical shape, which, after the near-field distance ($0.25{D_t}^2/\lambda$), starts to spread, forming a conical shape (Figure 2a,b) with an opening angle (φ). This beam opening can be estimated using the equation $\varphi = 29.5\lambda/D_t$ [38]. Note that the representation of the acoustic beam pattern given in Figure 2 is an oversimplification of the real

pattern, which is far more complex and, as an alternative, could also be assumed Gaussian [36,38]. The signal is strongest in the center of the beam pattern, also known as the central lobe. At larger angles, the intensity of the returned signal diminishes at usually 6–14% of the slant distance to the sediment bed (R) of central intensity, and the so-called first side-lobe appears. This intensity can mask the signal at the signal of the central-lobe and induce an error in further processing. The distance z_c (Figure 2b) depends on the incidence angle (θ) and beam opening (φ) and is denoted as the beam focusing height, related only to the central lobe [26]. Similarly, the side-lobe contaminated area is determined, and this zone is also known as a blank region because the velocity data are very noisy and not used for water velocity estimations [37]. Thus, the monostatic acoustic geometry is limited in the measurements close to the bed not only because of the side-lobe interference but also because of the uneven sampling of the acoustic pulse at the outer and inner boundary of the central-lobe. The acoustic footprint or the sampling area at the sediment bed (Figure 2a,b, D_s is the major axis of the ellipse) of the monostatic transducers can be assumed as an elliptical shape, calculated as given by Rennie et al. [17]. The uneven acoustic sampling of the sediments depends on the specific acoustic parameters (Table 2) and the signal-processing configuration. It enhances the influence of the strong surface scattering, resulting in erroneous echo intensities and Doppler velocity estimation [14,25].

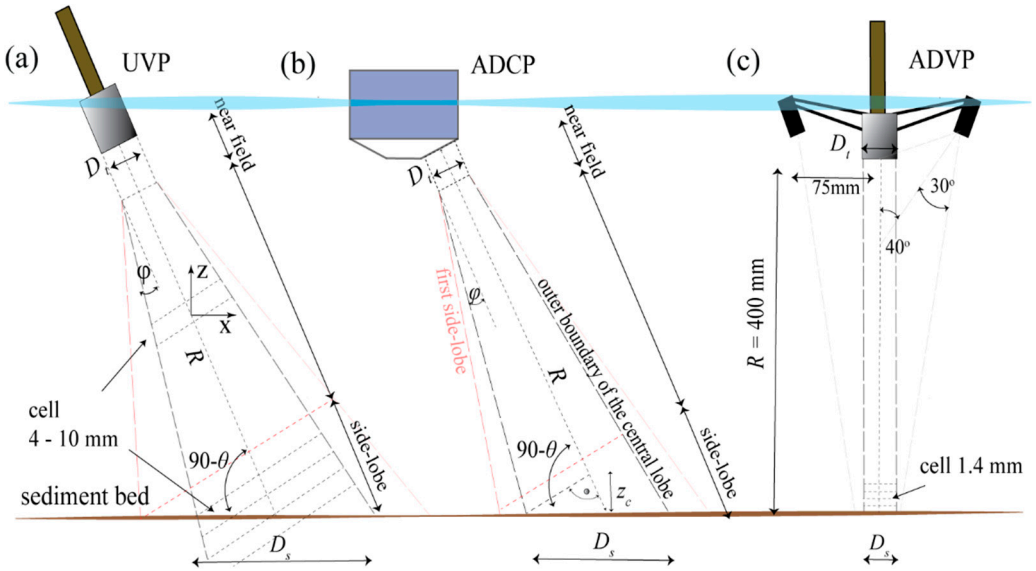

Figure 2. Acoustic geometry. (**a**) Acoustic Doppler velocity profilers (ADVPs)—Ubertone; (**b**) UVP—Ubertone; (**c**) ADCP Stream Pro—RDI.

The deployed UVPs in this study are monostatic transducers tilted in the direction of the flow and used to determine the mean velocity (i.e., for filtered turbulent oscillations) along the flume longitudinal direction (e.g., x in Figure 2a). To obtain an accurate estimation of the mean velocity, the assumption of the flow direction is crucial; therefore, it only applies in laboratory conditions. The minimum optimal measurement cell was chosen for the UVPs by adjusting the PRF and pulse length (Table 2). The ADCPs consist of four monostatic transducers arranged at 90° azimuth intervals. The transducers form acoustic beams at 20° for SPro (see θ, Table 2). The tilted beams enable the estimation of the velocity in the three directions (e.g., x, y, and z) under the assumption that the velocity is homogeneous in all four acoustic footprints. It is important to mention that, in this study, the BT feature of the SPro was used to measure the bed velocity. The BT feature utilizes longer pulses because they contain more energy, enabling deeper penetrations into the water column but also through the loose bed. Teledyne RDI (www.teledynemarine.com/rdi) created an algorithm [37] to identify the riverbed and estimate the BT velocity, which is not available for users, based on the same applied principle of detection of the maximum echo through a search over the echo profile found in the UVPs [37].

2.2.3. Bistatic Sonars

Bistatic sonars overcome some of the limitations of the monostatic by separately using an emitter and two or more receivers. This permits instantaneous measurements in two or more directions without any assumption for the flow direction. The side-lobe effect is also avoided, and the measurements can be obtained until the maximum fixed range of the instrument. These advantages come together with the limitation of having a fixed maximal ranging distance, which corresponds to the converging position of the projected and received beams. The central emitter forms a narrow vertical beam. The scattered intensity is then received at the two opposite wide opening angle receivers (±30° to the receiving beam axis). The receiving paths lay in the same plane of the emitted beam by forming ±40° angles with the vertical. The beams of the emitter and receivers must intersect (Figure 2c) in order to have measurements in more than one direction. Thus, the maximum range (R) of the bistatic transducers is determined by the distance between the transducers (75 mm from emitter to receiver) and beam opening (±30°), which has to be wide enough to cover sufficient distance in front of the transducer [27]. This maximum range is 400 mm for Ubertone's ADVP, which limits its application to field case studies. The projected beam pattern can be assumed as cylindrical, but after the near field, it also turns conical, and the cell size slightly changes as the depth increases. The definition of the cell is determined by the intersecting geometry defined by the receivers and emitter, typically explained by assuming ellipses that have foci at emitter and receivers [27].

The cell deformation at the end of the measurement range (R) the bistatic geometry provides an equal spatial distribution of the pulse scattering, eventually permitting profiling of the bedload velocities through the active layer, without significant influence of the immobile bed below [13].

The ADVP by Ubertone used in this study is a bistatic active sonar that has two receivers permitting the measurement of instantaneous velocity components in two directions (x and z, Figure 2c). The combination of the maximum range (Table 2) and the PRF accounted for smaller measurement cells (1.4 mm) than the UVPs and a better acoustic sampling at the sediment bed.

2.2.4. Echo Intensity (EI)

The echo intensity profiles (EI) are simultaneously measured with the velocities at each sample for both the bistatic and monostatic instruments used in this study. The backscattering strength (B_s), which actually depends on the sediment concentration and particle size distribution (PSD) [35], can be derived from the sonar equation and adapted for the bedload measurements as given by Conevski et al. [26].

$$B_s = 10log(S_s + S_v) = -SL + k_{dB}(EI - E_r) - A_f + 2\alpha R + 20log(R) - P_{dB}, \quad (1)$$

B_s typically decreases as the measurement is further away from the transducer due to the attenuation (α) of the ultrasound and spreading (20log(R)) of the beams at a slanted distance R, which is known as transmission loss (TL). The attenuation can be caused by the diffusion of the ultrasound by the sediment particles and due to the viscous absorption of the water. In both studies, the distance to the sediment bed was kept constant, and no suspended sediment was observed in the water column. Thus, the only change in the BS strength could be associated with bedload mobility. Although it is strenuous to analytically separate the volume (S_v) and the surface scattering (S_s), it is crucial to distinguish between the S_v that is induced by the mobile active layer of the bedload, whereas S_s is characterized by the strong scattering of the surface formed by the immobile particles beneath. The change of the size of the acoustic footprint area (A_f) caused by pulse length change, pitch and roll of the device, and eventual deformities of the bed could also influence the B_s [26]. The sampling area is relatively small compared to the observed bedforms in this experiment; thus, A_f *is* assumed to be constant. The source level (SL) and noise level (E_r) are also assumed to be constant. The UVPs use dynamic gain, which can change the SL automatically between 20 and 68 dB. The transmit voltage P_{db} is also constant because all instruments worked on a constant current supply.

Considering all these assumptions for the BS strength, it could be noticed that only the *EI* influenced the variability of B_s; thus, only *EI* was used in further analysis.

2.3. Data Postprocessing

2.3.1. ADCP Data Postprocessing

In both experiments, the ADCP was in a fixed position during the measurements; thus, the BT velocity was assumed to be equal to the apparent bedload velocity ($v_a = v_{bt}$). Although the SPro internally averages velocities obtained by several pulse pairs, the velocities measured close to the bed were prone to noise and had to be filtered. Filtering discards all velocities that are in the opposite direction of flow and the velocities that exceed three times the standard deviation of the velocity time series [14]. The final v_a is an average value of the filtered velocities. The partition of data that was filtered out (*FD*) is given as a percentage of the total ensembles collected during one repetition. For a more reliable comparison, only two beams were used, which were directed in the direction of the flow and assumed a two-dimensional flow in the flume and vertical directions similar to the ADVP.

The echo intensity (*EI*) of the ADCP data or the Receiver Signal Strength Indicator (RSSI), represents a value in the center of the bottom. The echo is despiked and averaged.

2.3.2. Detection of the Immobile Bed and the Cells Containing Bedload Velocities (Ubertone Instruments)

Both the UB-LabX and the ADVP by Ubertone are primarily designed to measure water velocities and do not have an internal algorithm to identify a solid surface or a sediment bed; therefore, a custom-made algorithm was developed. The bedload is characterized by complex two-phase scattering initiated by the mobile and immobile or potentially mobile bedload particles [14]. As explained in the previous sections, the scattering of the mobile particles in the active bedload layer depends on the form, shape of the particles, and the total concentration per unit volume, which induce volume scattering. Volume scattering of the bedload particles should be stronger than the scattering of the suspended particles in the water column (the outer region in Figures 3b and 4b) because of the higher concentration and larger diameter. Therefore, the first peak in the echo profile can be identified at a depth when the active bedload layer begins (first peak (FP) in Figures 3b and 4b). By applying the first derivative on the entire profile, the cell with that sudden change in echo can be identified. On the other hand, beneath the mobile bedload, the cells contain the scattering of the immobile particles from a rough surface that typically scatters much stronger. The signal is fully reflected from the rough surface and therefore the echo profile showed the maximum peak (Max EI in Figures 3b and 4b) in one of the cells. It is worth noting that the material below the active layer is very loose with high porosity, and this boundary is difficult to define. However, the concentration of the active layer is far lower than the substrate beneath. By using the first derivatives and cut-off amplitudes, it was possible to detect the range of cells that contain bedload data. Before applying the algorithm, despiking was necessary, and the use of an arbitrarily chosen cut-off amplitude was required because the presence of erroneous high EI in the upper part of the echo could lead to false identification of the sediment bed. Afterwards, the zero velocity values (i.e., no measured cells) were eliminated, and the data were further processed depending on the instrument (ADVP or UVP).

2.3.3. UVP Data Postprocessing

The inclined UVPs (Figure 1a) have delivered velocity profiles and echo intensities with different resolutions depending on the transducer's frequency (Table 2). The maximum range of all instruments was adjusted to reach the bottom; thus, the cells of the lower part of the profile contained information of the sediment bed (Figure 3). This adjustment influenced the resolution of the velocity profile, which also depends on the PRF and the instrument-carrying frequency. The maximum possible resolution for approximately 35 cm range up to the loose bottom resulted in a 4 mm cell size for the 1.5 MHz and 3 MHz and 10 mm cell for the 0.5 MHz, for both vertical and tilted beams.

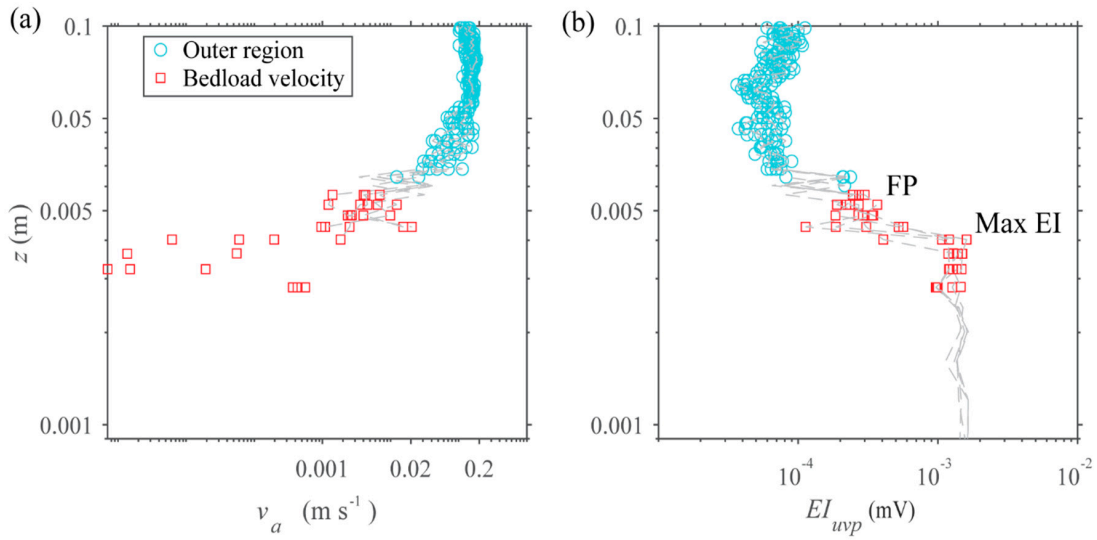

Figure 3. (**a**) Full velocity profile of UVP at 1.5 MHz, $\theta = 25°$; (**b**) echo intensity profile of UVP at 1.5 MHz, $\theta = 25°$.

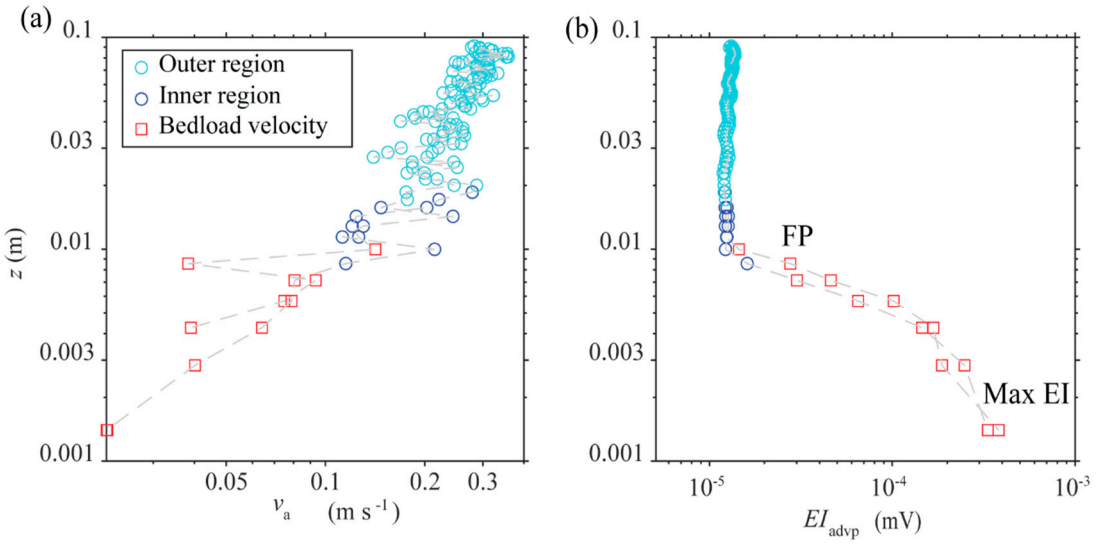

Figure 4. (**a**) Full velocity profile of ADVP; (**b**) echo intensity profile of ADVP.

The algorithm explained above searched for the first echo peak and the maximum echo (Figure 3b) in one instantaneous measurement (at 10 Hz). Due to the noisy data close to the bottom and the side-lobe mirroring, a cut-off amplitude, equal to the 0.5 Max EI, was used to filter out the false echoes.

By filtering the velocities in the flow direction [14], as explained in the previous section, it was concluded that only two to three cells out of all identified (red squares in Figure 3) were used to obtain reasonable apparent bedload velocities. One cell above and one cell below the first peak (Figure 3) were eventually considered to assess the mean bedload velocity derived from the UVPs. This also avoided contaminated cells from the outer region, which may affect the Doppler velocity close to the loose bed. The inclined monostatic geometry has an uneven acoustic sampling of the sediment bed, which means that the measurement cells were not fully covering the bed (Figure 2b). The active layer thickness may vary during one sample. By performing trial-and-error analysis, it was observed that the best result or the best correlation was obtained by analyzing a minimum of three cells (at 1.5 MHz and 3 MHz). A total cell thickness of 12 mm at 1.5 MHz and 3 MHz and 20 mm for the 0.5 MHz was considered for sampling the sediment bed. In this way, the acoustic resolution covered the maximum saltation height of the bedload particles, including the height of the bedforms in the sampling area.

Finally, the time series of velocities (v_a by UVP) for each repetition was time-averaged and used for analysis in this study.

The echo intensity (EI_{uvp}) of the UVP data is given in mV and only despiked and time-averaged.

2.3.4. ADVP Data Postprocessing

The ADVP output is in blocks that are 3 min of instantaneous profiles for three different configurations characterized by changing profile and time resolution. Given the objective of this paper, herein, the results from maximum resolution profiling are considered. Instantaneous velocity profiles are available with a frequency of 5–7 Hz. The maximum range and distance to the sediment bed of about 35 cm resulted in a 1.4 mm cell size resolution.

To detect the sediment bed, the same algorithm was used, which was explained in the previous section for the monostatic UVP. Contrary to the monostatic instrument, the bistatic instrument does not have limitations in acoustic sampling. The cells are equally distributed and almost parallel to the sediment bed [25]. Therefore, the velocities of each cell were considered as the unique value of the bedload velocity profile (red square symbols, Figure 4a). The cell below the first peak is assumed as the beginning of the active layer, whereas the maximum depth cell is considered as the fully immobile loose bed (Figure 4b). The number of cells used for the bedload velocities depended on the transport conditions and the active layer thickness. However, it is expected that cells in the upper part of the detected layer would be strongly influenced by the water velocity due to the extremely low particle concentration at these shallow cells. The lower set of measurement cells (one cell up and below the Max EI) would be influenced by the strong surface scattering.

Despite the better accuracy and acoustic sampling, the obtained instantaneous velocities were extremely noisy, which required despiking using threshold value from the water velocity profile and, finally, time averaging. In detail, the obtained velocities (v_a, by ADVP) time series at each cell were averaged over three minutes block, and these time-averaged values were compared with the ADCP and the camera results. The values measured at Positions 1 and 2 (Figure 2a) were analyzed separately to avoid a possible spatial variability of the sediment transport during one repetition.

The echo intensity (*EI*) was also despiked and time-averaged. Different dynamic echo gains were noticed in the two hydraulic conditions (EXP1 and EXP2) in the UniBo flume; therefore, the *EI* from different experiments could not be explicitly compared.

2.3.5. Imaging Data Postprocessing

The GoPro cameras are equipped with wide-angle lenses that are known for their fish-eye effect. This distortion was corrected by applying an algorithm designed to undistort the images. To compensate for other distortions and determine the calibration parameters, several images of a calibration checkerboard were taken in underwater conditions. Note that in underwater conditions, the light refraction changes significantly, and thus the field of view and distortion decrease (e.g., 135° to 95° for GoPro lenses).

The imaging data had to be preprocessed to enhance the pixel intensity, deblurring, and sharpening. After that, the mobile particles were located using a two-frames change detection algorithm, as detailed in Conevski et al. [14,26]. Additional filters were applied to the differenced images to eliminate the false background and false foreground pixels [26]. The next steps followed a typical particle image velocimetry methodology, including division in region of interests (ROI) and cross-correlation performed at the subsequent pairs of differenced images [12]. The latter provided the camera velocity (v_c), which is assumed to be the velocity of the particles moving at the top of the active bedload layer. The raw pixel/frame velocities were converted into SI units, and the data were despiked. The differenced images, which detect particle displacement, also allowed calculating the surface concentration of bedload transport (*K*). Since the bedload active layer thickness can reach ten times the D_{50} for sand [33], *K* is thus assumed to be the surface bedload concentration, not considering a variation in depth.

3. Results

3.1. Apparent Bedload Velocities—UniBo Experiments (ADVP vs. ADCP)

The postprocessed data measured simultaneously by the ADCP and ADVP were averaged and compared for each experimental repetition for both positions (Figure 2a). The averaged values of all repetitions are shown in Table 3. The apparent bedload velocities and the echo intensities (*EI*) measured both by the ADCP and the ADVP did not differ between Positions 1 and 2, which showed the spatial homogeneity of the bedload transport throughout the flume. This allowed comparing the instrument outputs regardless of the position and repetition.

Table 3. Average bedload data measured at two positions in the UniBo flume, Qs^m is the sediment transport rate measured by a bedload trap.

EXP		SPro		Camera		ADVP	
	Qs^m	v_a	*EI*	v_c	*K*	v_a	*EI*
35 cm to BED	g s^{-1}	m s^{-1}	dB	m s^{-1}	/	m s^{-1}	μV × 10^{-3}
EXP1 POS1	2.46	0.006	62.2	0.07	0.35	0.035	0.18
EXP1 POS2		0.005	62.2			0.040	0.17
EXP2 POS1	12.63	0.014	62.5	0.11	0.55	0.055	0.41
EXP2 POS2		0.014	62.3			0.058	0.45

The ADVP resolution of 1.4 mm cell size permitted analyzing the bedload velocity and defining a velocity profile of the active bedload layer. For EXP1, six cells above the immobile sediment bed (i.e., Max EI) were analyzed, and for EXP2, eight cells were predefined by the algorithm (Figure 4). The total height of six to eight cells corresponds to 8–11 mm, which was in the range of the maximum saltation of particles with a median diameter of 1 mm [33].

Figure 5 shows the profile of velocities measured at different distances from the fully immobile sediment bed (i.e., Max *EI*). The blue symbols are representing the cells around the first peak (FP) or the cells that measured the upper part of the active layer. The range of the camera velocities (v_c) for both experiments was in the range of the top cells measured by the ADVP profiles given in Figure 5, implying that the top cells measured the water velocities, with the small influence of the particles that were entrained in the water column. Note that the planar view of the camera was only able to capture the topmost layer of the bedload [14].

The red symbols in Figure 5 are the velocities computed from cells that most likely sampled the immobile sediment bed. These cells had zero velocities or negative values (i.e., the opposite of the flow direction) caused by the surface scattering (Figure 5a), which was even more obvious for the EXP1 due to the weaker transport. For EXP2 the maximum echo probably did not reach the fully immobile particles due to the abundant bedload transport, and relatively higher bedload concentration (*K*, Table 3).

Figure 5 clearly shows that the bedload active layer started one cell below the top cells (blue circles in Figure 5b and cyan circles in Figure 5a); thus, the real mean bedload velocity given in Table 3 was calculated by averaging all this data until the last cell. Note that this cell was included because some of the particles might be mobile and rolling in addition to the despiking of the data that eliminated eventual erroneous data.

As the measurement cells approached the immobile sediment bed, the measured velocities by the ADVP started to match the ADCP apparent velocity (Figure 6). The SPro measured in profiles with a fine resolution that actually was strongly influenced by the surface scattering that resulted in a high percentage of erroneous data (*FD*) and underestimated 3–8 times the surface bedload velocity (i.e., v_c) [14]. This is in agreement with the results presented by Conevski et al. [26], which confirmed

that the surface scattering and the instrument resolution are the main factors for the underestimation of the bedload velocity and for producing erroneous data.

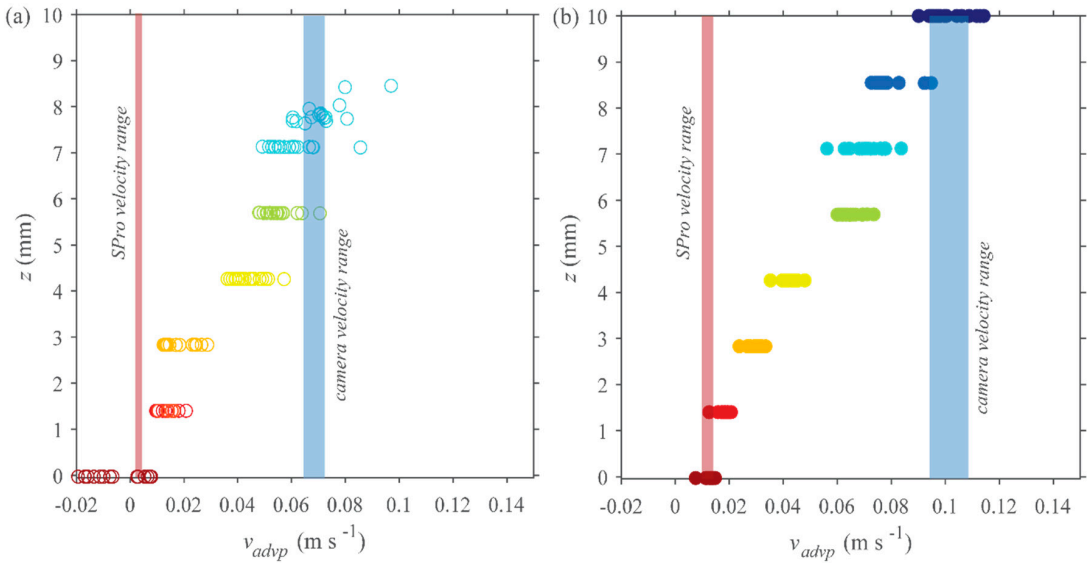

Figure 5. UniBo bedload velocity profiles measured at both position and the range of ADCP SPro and camera velocities (**a**) EXP1, weaker transport conditions, U = 0.42 m s^{-1}; (**b**) EXP2 intensive transport conditions, U = 0.58 m s^{-1}.

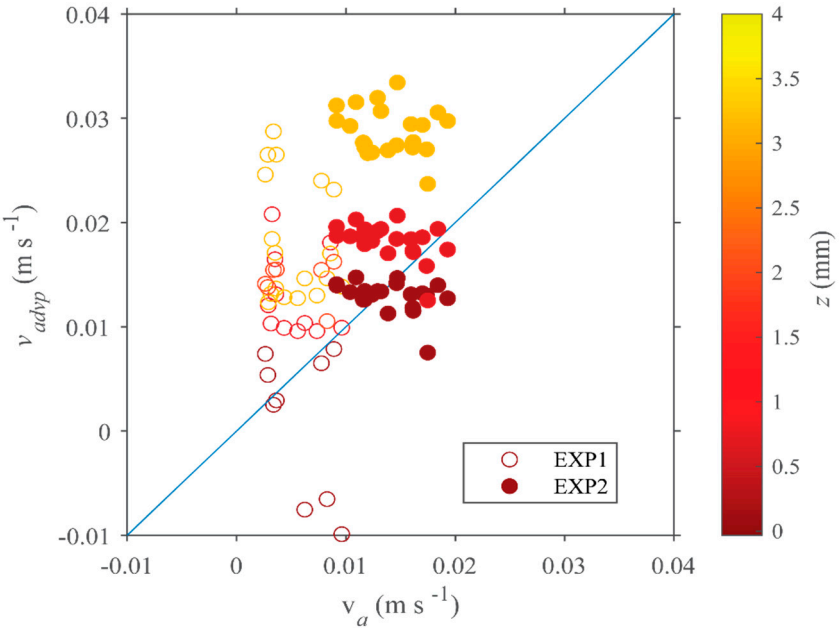

Figure 6. ADCP vs. ADVP velocities in the last three cells close to the immobile bed, and z is the distance to the immobile sediment bed (e.g., z = 0). The dark red color of the colormap symbolizes the immobile sediment bed.

3.2. *Apparent Bedload Velocities—NTNU Experiments (UVP vs. ADCP)*

For the NTNU experiments, only the set of the tilted transducers were able to measure the bedload velocities in the direction of the flow. The data measured by the three UVPs transducers (3 MHz, 1.5 MHz, and 0.5 MHz) is averaged and filtered in the water flow direction, including a cut-off velocity that excluded the eventual measurements in the water cells. The mean values in Table 4 show that the velocities observed by all three frequencies are different. The lowest apparent

velocity value was measured by the lowest frequency and resulted in eight times for sandEXP1 and five times, for sandEXP2, a lower velocity than the surface bedload velocity (v_c) measured by the camera (Figure 7a). On the other hand, it fully matched with the velocity measured by the SPro in sandEXP1 (Table 4). The latter demonstrated that both the SPro and the 0.5 MHz frequency were strongly influenced by the surface scattering, giving lower velocities. For the SPro, the BT algorithm is not open for the users, but by using BB coded element signal processing, it can be assumed that the cell used to estimate the bedload velocity was fully covering the sediment bed. A similar situation could be stated for the 0.5 MHz transducers, but here, even if one cell (10 mm) was fully covering the sediment bed, the other cell located above it was also considered in the average value, which apparently did not influence the result. In addition, the sand with a 0.35 mm grain size was scattered in the Rayleigh scattering regime [38], which embodied lower energy in the volume scattering by the bedload particles that caused lower *EI*. This may have induced problems in the echo autocorrelations and the estimation of the apparent velocity [25].

Table 4. Average bedload data measured in the NTNU flume. Qs^m is the sediment transport rate measured using the bedload trap.

EXP	SPro			Camera			0.5 MHz		3 MHz		1.5 MHz	
	Qs^m	v_a	*EI*	v_c	*K*	d_t	v_a	*EI*	v_a	*EI*	v_a	*EI*
35 cm to BED	g s^{-1}	m s^{-1}	dB	m s^{-1}	/	mm	m s^{-1}	μV × 10^{-3}	m s^{-1}	μV × 10^{-3}	m s^{-1}	μV × 10^{-3}
sandEXP1	0.00	0.002	57.9	0.02	0.06	0.53	0.002	0.45	0.005	0.11	0.01	0.39
sandEXP2	/	/	/	0.05	0.12	/	0.010	0.65	0.022	0.93	0.035	0.91
sandEXP22	0.49	0.007	57.5	0.08	0.20	2.26	/	/	/	/	/	/

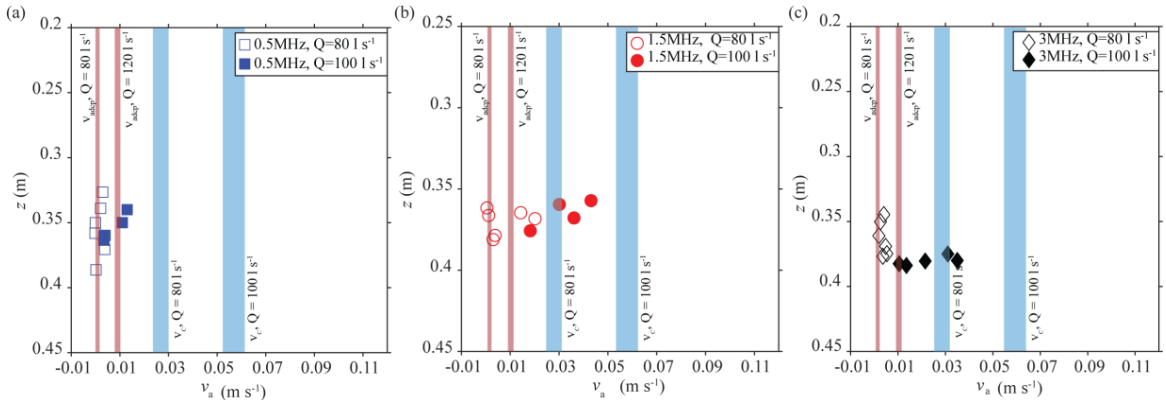

Figure 7. Bedload velocities measured by the tilted UVPs for both conditions, Q = 80 l s^{-1} and Q = 100 l s^{-1}: (**a**) 0.5 MHz; (**b**) 1.5 MHz; (**c**) 3 MHz.

On the other hand, the transducer working at 1.5 MHz provided the highest apparent bedload velocity that almost matched the camera's observed values (Figure 7b). This implies that the 1.5 MHz transducer was less influenced by the surface scattering and observed relatively accurate velocities of the bedload particles. It was expected that the higher frequency would deliver the highest bedload velocity and the most superficial sampling due to a possible higher attenuation in the active layer. Although the transducer working at 3 MHz frequency had the same cell size as the one working at 1.5 MHz, it resulted in velocities 2–3 times lower than the 1.5 MHz transducer and the imaging data (Figure 7c). One reason for this was the shorter penetration and maximum range of the higher frequencies (e.g., 3 MHz, Table 2), resulting in fewer cells sampling the active layer from top to bottom, which stemmed in lower accuracy of the flume bed identification.

Interestingly, the bedload velocity measured by all UVPs for the sandEXP1 was in the range of the SPro, implying that in the weak transport conditions, the measurement error is higher and the surface scattering is stronger.

However, the main source for bedload velocity underestimation of the monostatic systems is the actual sampling of the mobile sediment bed. Thus, the smaller beam opening angle (φ) of the 1.5 MHz transducers contributed to (i) a low effect acoustic beam outer region, (ii) a more superficial sampling, and (iii) less influence of the surface scattering but a larger acoustic footprint area (D_s). Note that the camera velocity is the velocity of the topmost bedload particles; thus, the 3 MHz transducers might have given the most realistic mean bedload velocity.

Similarly, as discussed by Conevski et al. [25], Figure 8 illustrates the influence of the pulse length (Pl) and the acoustic beam geometry on the bedload velocity measurements. The larger the ratio D_s/Pl, the shallower the acoustic sampling and the higher the value of the velocities as a physical consequence.

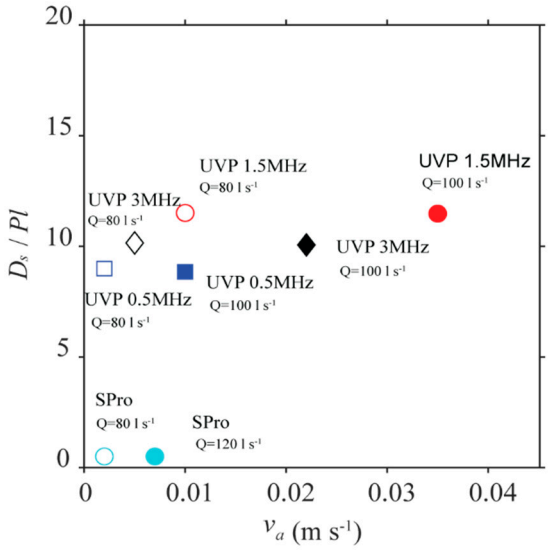

Figure 8. The influence of the monostatic acoustic geometry and sampling in the bedload measurements.

Note that for the UVPs and short-ranging distances, such as in the flume experiments, D_s/Pl almost corresponds to the ratio of 1/φ except for a vertical beam (Table 2). This occurrence corroborates previous findings regarding the effect of the outer boundary of the central lobe (Figure 2b) on the acoustic sampling and apparent velocity [25]. Similarly, wide opening angles contribute to a stronger influence of the inner portion of the main acoustic beam. The resulting apparent velocity is reduced because of the faster return of the acoustic signal reflected in these regions. In addition, longer pulse lengths increased the thickness of the acoustic sampling at the flume bottom and were partially reflected by the fixed particles beneath the bedload layer (i.e., surface scattering). A more focused beam and shorter pulse length resulted in greater measurement resolution at the flume bed, which provided higher apparent velocity because of the prevailing volume scattering from moving particles at shallower depths. The deepest sampling and the long BT pulses of the SPro significantly contributed to a strong influence of the surface scattering beneath the bedload layer and the lowest velocities observed (Figure 8). In the same manner, the major axis of the sampling area D_s is calculated by a trigonometrical combination of the acoustic geometry parameters, including the grazing angle, the opening angle, and the diameter of the transducer. The SPro had the largest grazing angle ($90° - \theta = 70°$); thus, the impact of the surface scattering is expected to be stronger, which again, contributed to small apparent bedload velocity per each experiment. It is worth noting that larger grazing angles tend to be less sensitive to volume scattering, and for the grazing angle equal to 90° (i.e., vertical beams), the apparent velocities are not measurable. The SPro signal modulation is quite different from the UVPs' two-pulse coherent method. This certainly influenced the acoustic sampling [25] and provided unaligned marks in Figure 8 by using the simplified parameter D_s/Pl.

3.3. Deviation in the Bedload Velocity Estimation: UniBo Experiments (ADVP vs. ADCP)

The bedload velocity (v_a) measured by the ADVP given in Table 5 is the mean of six cells for EXP1 and eight cells for EXP2. The standard deviation (STD) of the ADVP in Table 5 is the average of the STD calculated for each of these cells. The deviation of the bedload velocity for the ADVP was in the range of the mean bedload velocity (Table 5), which is caused by the nonhomogeneous motion of the bedload particles. Although the PSD was well-sorted, the measurement cells might contain zero or several particles with different shapes and instantaneous velocities at different instances. This sporadic nature resulted in a wider range of velocities of the bedload particles [9,14] and somehow challenged the bistatic configuration feature, which theoretically made it possible the two-dimensional instantaneous measurement of the Doppler velocity. In other words, instantaneous measurement of bedload velocity appeared hardly possible because of the random and noisy nature of the investigated process close to the flume bed, although the bistatic configuration made available two components' velocity at the same instant. The relatively high variation of the bedload transport velocities was also present in the ADCP data, despite that final bedload velocity was underestimated by a factor of two or three. The STD of the SPro calculated from the raw data, before applying despiking and filtering (i.e., *beforeSTD*v_a in Table 5), was 10–20% higher than the mean apparent velocity. The filtered data (*FD*) of the SPro decreased by 10–15% for EXP2 as the bedload transport condition became more intensive, which accounts for less penetration of the signal and less influence of the surface scattering [14].

Table 5. The apparent bedload velocity variability in the UbiBo experiments.

EXP	ADVP			SPro				
	v_a	*STD*v_a	*repSTD*v_a	v_a	*beforeSTD*v_a	*STD*v_a	*repSTD*v_a	*FD*
	m/s	m/s	m/s	m/s	m/s	m/s	m/s	%
EXP1 POS1	0.035	0.0400	0.0030	0.007	0.006	0.003	0.0023	49%
EXP1 POS2	0.04	0.0510	0.0050	0.006	0.005	0.003	0.0025	59%
EXP2 POS1	0.0545	0.0480	0.0040	0.014	0.012	0.009	0.0020	43%
EXP2 POS2	0.058	0.0510	0.0040	0.014	0.011	0.007	0.0031	40%

On the other hand, the STD between the experimental repetitions (i.e., *repSTD*v_a in Table 5) of the measured bedload velocity for both ADVP and ADCP was low and almost constant (Table 5), which again demonstrates the repeatability of the simulated conditions.

3.4. Deviation in the Bedload Velocity Estimation—NTNU Experiments (UVP vs. ADCP)

The STD, for all UVPs, obtained from the raw data (i.e., *beforeSTD*v_a in Table 6) was three to five times higher than the estimated mean, which was a consequence of the relatively high number of spikes, which contaminated the cells closer to the water column. The high STD of the raw data made clear that the postprocessing (i.e., threshold filtering) is a key step in the ultrasound bedload measurements.

At the same time, the filtered data (*FD*) of the UVPs were lower than the SPro measurements. Additionally, 15–20% of the data were discarded data for the sandEXP1 and 20–30% for sandEXP2 for all the UVPs (Table 6), regardless of the different mean velocities (v_a). The *FD* values for the UVPs increased for the more intensive bedload conditions (sandEXP2) because of more diffusive bedload transport and more irregular bedforms. Moreover, the STD of the apparent bedload velocity after the filtering for all UVPs also decreased. Note that the UVPs used very short pulses and some of the cells did not have full contact with the immobile bed, which contributed to low *FD*. This was not the case for the SPro because the internal BT detection algorithm searched for the immobile particles and most likely

the topmost layer of the active bedload was not efficiently sampled. In addition, the pulses used by the BT feature are much longer than the UVPs, enabling more energy and longer contact with the sediment bed. This deep contact with the immobile bottom affected the Doppler velocity estimation resulting in 80% erroneous data. The *FD* was higher than the experiments at UniBo, potentially associated with stronger scattering of the coarser sand particles at UniBo tests, which eventually resulted in better estimation of the apparent velocity. The *FD* for SPro decreased with increasing transport because the active layer was thicker in more intensive conditions and the bedload concentration was higher, which resulted in shallower detection of the bottom cell. Thus, the echo from the immobile surface was less present, and fewer errors appeared in the apparent bedload velocity time series.

Table 6. The apparent bedload velocity deviation in the NTNU experiments.

EXP	0.5 MHz						1.5 MHz				
	v_a	*before* $STDv_a$	$STDv_a$	*repSTD*v_a		*FD*	v_a	*before* $STDv_a$	$STDv_a$	*repSTD*v_a	*FD*
	m s^{-1}	m s^{-1}	m s^{-1}	m s^{-1}	%	m s^{-1}	m s^{-1}	m s^{-1}	m s^{-1}	%	
sandEXP1	0.002	0.0065	0.0054	0.0015	17%	0.01	0.0514	0.0077	0.0016	9%	
sandEXP2	0.01	0.0306	0.0119	0.00025	21%	0.035	0.0711	0.0345	0.0124	30%	
sandEXP22	/	/	/	/	/	/	/	/	/	/	
	SPro (2MJHz)						3 MHz				
	v_a	*before* $STDv_a$	$STDv_a$	*repSTD*v_a		*FD*	v_a	*before* $STDv_a$	$STDv_a$	*repSTD*v_a	*FD*
	m s^{-1}	m s^{-1}	m s^{-1}	m s^{-1}	%	m s^{-1}	m s^{-1}	m s^{-1}	m s^{-1}	%	
sandEXP1	0.002	0.001	0.0004	0.0001	80%	0.005	0.0409	0.0067	0.0014	19%	
sandEXP2	/	/	/	/	/	0.022	0.054	0.011	0.0042	28%	
sandEXP22	0.007	0.005	0.0040	0.0010	43%	/	/	/	/	/	

After the filtering of the bedload velocity data, both the UVPs and SPro provided standard deviations (i.e., $STDv_a$ in Table 6) within the range of the mean values, similar to the UniBo outputs.

A low deviation between experiment repetitions (i.e., *repSTD*v_a in Table 6) confirmed the reliability of the collected data.

3.5. Echo Intensity: UniBo Experiments

The echo intensity of the SPro was relatively constant for both conditions, with only a 0.3 dB decrease when passing from EXP1 to EXP2 (Table 4). By knowing that the RDI algorithm used static gain searches for the immobile bed at the best possible resolution [37], the small reduction could be a result of the attenuation of the signal due to the thicker active layer of bedload and irregular bed.

On the other hand, the ADVP in the same experimental set-up used a dynamic gain, which increased the signal intensity ruled by internal parameters, which were unknown for the users. Given the lower suspended particle concentration and acoustic return, the gain was most likely higher in the EXP1 and therefore the *EI* (given in µV) doubled the EXP2 value (Figure 9). For both experiments, the *EI* increased as the observed cells approached the immobile sediment bed (passing from blue to red marks in Figure 9), which was a result of the higher concentration of bedload in lower parts of the bedload layer. Moreover, the surface scattering might have some influence on the last measurement cells because of the sediment bed irregularity and partial sampling of the immobile particles beneath the active layer (i.e., the sampling area is over a ripple or dune). Interestingly, the *EI* of the last cells (triangle symbols in Figure 9) slightly diminished when compared to the cell above (a drop of 0.1 mV for EXP2 and 0.05 mV for EXP2). This decline is in opposition to the general trend of a larger return from deeper layers that made evident that sound attenuation occurs at irregular and a loose sediment bottom beneath moving particles.

Furthermore, the first cells (i.e., most shallow) of the EXP1 (cyan and light green empty symbols in Figure 9) and the first cell of EXP2 (dark blue full symbols in Figure 9) have almost the same values for the EI, which indicates that these cells were mostly sampling the water column where the moving particles have a weak effect in the absence of a suspended load.

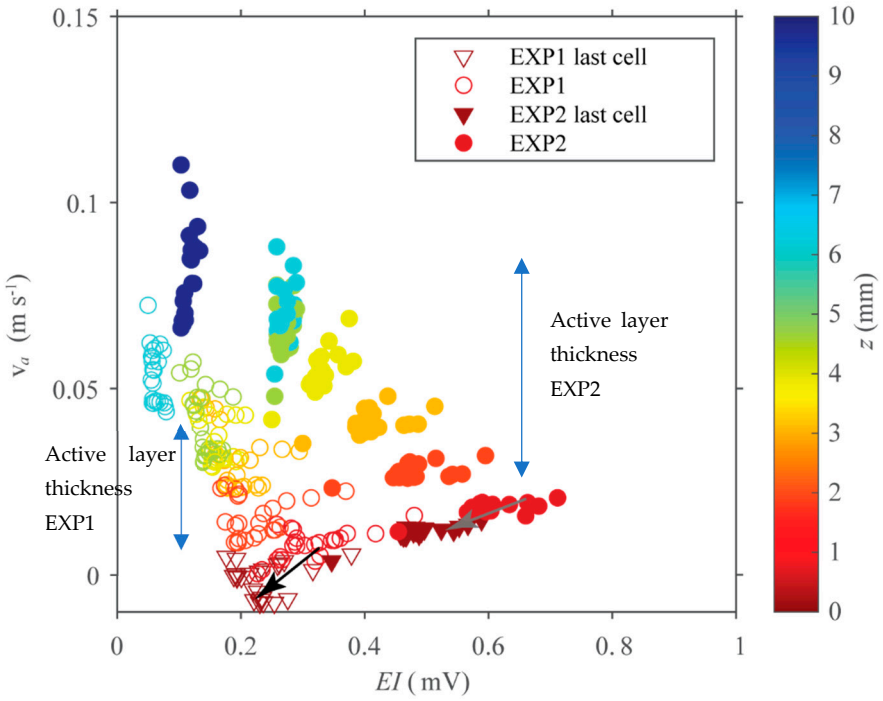

Figure 9. ADVP echo intensity throughout the cells close to the mobile sediment bed, z is the distance to the immobile sediment bed (e.g., z = 0). The black/gray arrows show the decrease of the amplitudes due to the surface irregularity and signal attenuation, passing from circle symbols to triangle symbols.

Moreover, the observed change of the *EI* gradient in the last upper cells and the last cell close to the bottom might be an identification of the active layer boundaries, hence the active layer thickness.

3.6. Echo Intensity: NTNU Experiments

The SPro BT mode uses long pulses, a relatively high cell resolution, and BB signal processing to identify the sediment bed [26]. The Doppler shift is determined from the cell corresponding to the sediment bed, which was used to determine the apparent bedload velocity and the echo intensity (Table 4). Similarly, as in the UniBo experiments, the *EI* stayed constant with a small reduction (0.3 dB) when passing to more abundant transport conditions.

In the same experimental set-up, the UVPs used short pulses, a high cell resolution, and PC signal processing. Two sets of measuring cells were observed to better analyze and compare the results from the backscattered signal. Figure 10a–c shows the average *EI* of the cells used to define the bedload apparent velocity (i.e., cell above and below the first peak-FP, Figure 3), and Figure 10d–f presents the cells corresponding to two cells above the MAX amp, which mostly represents the return from the immobile surface. The apparent bedload velocity was always estimated from the cells at the first peak. Note that in most of the samples/profiles, one of the cells analyzed in Figure 10d–f overlapped with the lowest cell used for the *EI* in Figure 10a–c because the immobile bed is placed below the active layer. Figure 10a–c represents the active bedload layer, without or with very little contact with the immobile surface. Therefore, the *EI* increased when passing from weaker to more intensive hydraulic conditions (Figure 10a–c, i.e., passing from Q = 80 l s^{-1} EXP1 to Q = 100 l s^{-1} EXP2), which is due to higher bedload concentration when passing to EXP2.

The *EI* measured by the vertical beams (i.e., V suffix in Figure 10a–f legends) is also presented in Figure 10a–c, and it stayed almost constant when passing from weak to abundant transport conditions. Although the bedload concentration was also higher the vertical beams are generally less sensitive to volume scattering and the *EI* negligibly changed [40].

Figure 10d–f shows the cells that were beneath the active layer and partially or fully covered the sediment bed for both inclined (θ = 25°) and vertically mounted UVPs; thus, the range of the *EI* is almost 50% higher than the return from the active layer (Figure 10a–c) for 1.5 MHz and 3 MHz. The results for the 0.5 MHz transducers for the tilted UVP show a lesser increase (compare Figure 10a,d) because the longer pulse length (i.e., the cell size) resulted in some overlap between the two identified regions. The *EI* for the vertical beams in both sets of cells (Figure 10a–c vs. Figure 10d–f) resulted in very similar values. In addition, the 0.5 MHz transducers most likely used different emitting source levels, which generally resulted in lower *EI* than the values for the 1.5 MHz and 3 MHz transducers. The higher frequencies used the same transducer type, whereas the 0.5 MHz was different. Furthermore, referring to the deeper region (Figure 10d–f) the *EI* slightly decreased for all tilted UVPs when passing from weaker to more intensive conditions (e.g., from empty to full symbols in Figure 10d–f). This is in contrast with the observed trend in the upper region (i.e., the active layer represented in Figure 10a–c) and corroborates the hypothesis of an attenuation effect when pulses pass through the bedload layer and reach the loose irregular bottom surface formed by the immobile particles.

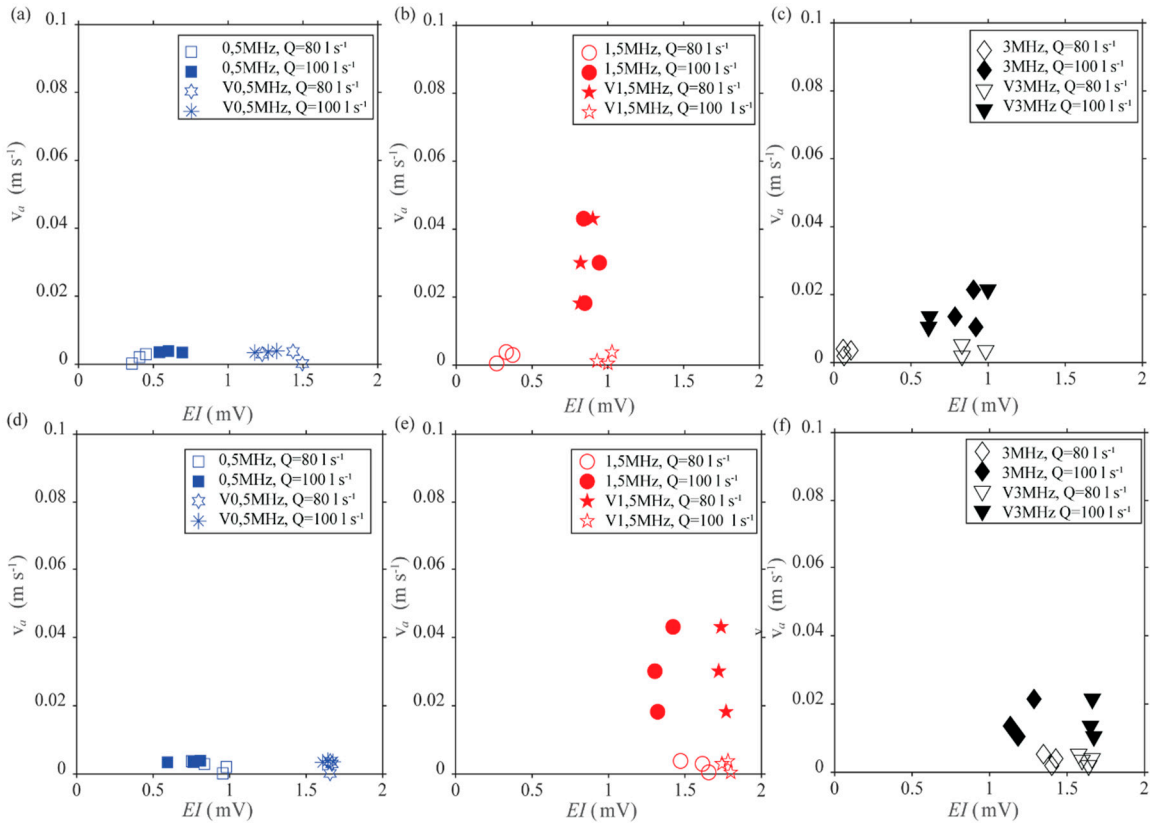

Figure 10. The echo intensity and the apparent bedload velocity measured by the UVPs at NTNU experiment. The V suffix indicates vertically aligned UVPs (ϑ = 90°,) whereas ϑ is 25° and not differently specified. For vertically aligned UVPs, no apparent velocity is available; therefore, it stays the same as measured by the 25° tilted UVP. (**a–c**) The 0.5–1.5–3.0 MHz UVPs with three averaged cells representing the active layer of bedload moving particles, which were used to estimate the apparent bedload velocity; (**d–f**) 0.5–1.5–3.0 MHz UVPs with two averaged cells above the MAX Amp value representing the loose bottom mostly formed by immobile particles beneath the active layer, which is consistent with the SPro algorithm for riverbed detection.

SPro backscatter (B_s in Table 4) was compared to *EI* from the deep region beneath the active layer, which identified the sediment bed more accurately and is consistent with the RDI BT internal algorithm for riverbed detection. The *EI*, for both SPro and tilted UVPs (Figure 10d–f), decreased in the range of 0.1–0.3 mV as the bedload transport intensity was increasing. Finally, as expected, the results from

vertical UVPs are constant for both bedload transport conditions due to vertical signal reflection from the immobile sediment bed and the less sensitivity to the volume scattering. In this case, the small deviations are associated with surface deformations caused by the bedforms.

4. Discussion

4.1. Apparent Bedload Velocity

Despite measuring only the velocities aligned in the flow directional velocities, the ADVP reliably measured the mean velocity of the rather nonhomogeneous and anisotropic nature of the bedload motion. The velocity profile showed that the planar imagery velocity (v_c) resulted in a slight overestimation of the true average bedload velocity, which was calculated as the mean of the bedload velocity profile obtained by the ADVP [14]. In the same context, the normalized apparent bedload velocity (v_a/K) measured by SPro resulted in a value two-fold lower than the true bedload velocity for both bedload transport conditions. This improved the results presented by Conevski et al. [14], who stated that the normalized apparent velocity from SPro is underestimated by two to five times. This indicates that, given the same acoustic sampling, the ADCP would systematically underestimate the bedload velocity, enhancing easier calibration, especially when applying the kinematic transport model [18,25], It is worth noting that in large rivers with depths more than 2 m, ADVP deployment appears challenging, and its improved resolution should play a less relevant role in repairing the acoustic sampling due to the larger measurement of cells and small variations in the sampling volume. An averaging time of a few minutes was required to eventually filter and despike the ADVP profiles. This postprocessing step remains key to eventually obtain time-averaged consistent estimations of bedload velocity. The same is valid for ADCPs [14]. The instantaneous measurement of two components of the velocity is made possible by bistatic configuration; however, this appeared poorly relevant for taking bedload measurements. This was the case of experimental conditions characterized by a low quality of instantaneous profiles inherent from the investigated process' randomness and low scattering environment.

The monostatic systems demonstrated that acoustic sampling, which combines beam geometries with signal modulation (e.g., the pulse length), also plays an important role. The 1.5 MHz transducer measurements corresponded to the top of the active layer velocities (i.e., camera velocity). The 3 MHz transducer, although with the same resolution, provided half the velocity of the camera, which is most likely equal to the averaged bedload velocity, and the 0.5 MHz transducers provided velocities in the range of the SPro system, an underestimation of five to eight times the camera velocity and two to five times when the normalization is applied (v_a/K). These results demonstrated that by changing the parameters of the transducer (such as diameter, frequency, distance to the bed, and resolution), the acoustic sampling and estimated apparent bedload velocity could result in different positions within the active layer. It is most likely that the low-frequency sonar (0.3 MHz–1 MHz) was able to adjust for more superficial acoustic sampling due to the problem of aliasing and echo ghosting, which constrains the PRF—max velocity/distance parameter tuning. The higher frequencies of 1.5 MHz and 3 MHz affirmed that the correct parameter adjustment could result in accurate bedload velocity. However, the so-called water bias [19] and the ability to attenuate faster would be a serious restriction in field applications.

It must be noted that for both monostatic and bistatic configurations, the cell corresponding to the first peak (FP in Figures 3 and 4) did not necessarily represent the top of the active layer. The bistatic configuration case was simpler because: (i) the acoustic sampling was equivalent through one measurement cell, which resulted in less noisy data; (ii) the resolution was finer. However, it was not possible to determine which of the first three cells was the actual mobile bedload. For the monostatic configuration, it was even more troublesome to choose only one cell to represent the bedload velocity because one measurement cell (4 mm for 1.5 MHz) corresponded to 80–100% of the height of the active layer (~0.4–6 mm). Despite the full coverage of the mobile active layer by one cell,

the tilted acoustic geometry (Figure 2b) permitted three cells to partition the sampling of the sediment bed (Figure 2b) [26]. As a result, the UVP profiling of the bedload was somewhat comparable to the ADCP acoustic geometry, although the echo gating (i.e., measurement cell) was unknown for the ADCP BT feature. This implies that the higher apparent bedload velocity obtained by the 1.5 MHz was not only an outcome of the analyzed cells at the top of the active layer but should also the weaker surface scattering (e.g., shallower acoustic sampling), which eventually produced less noisy data in the cells of interest. Note that this choice was made by trial-and-error analysis. Different adjustments may be required in another experimental set-up depending on the transducer, distance to the bed, and carrying frequency.

In both experiments and for both configurations, it was clearly shown that the presence of surface scattering in acoustic sampling resulted in erroneous bedload velocities. These were particularly highlighted by the ADVP profiling of bedload velocity close to the loose bed, formed by almost immobile bedload particles and placed beneath the active layer. This produced negative velocities that corresponded to the results obtained by the SPro system.

4.2. Echo Intensity

The comparison of the echo intensity data was more problematic due to the dynamic gain setting of the Ubertone instruments (e.g., ADVP and UVP). The dynamic gain increases the *EI* when there is a loss of signal strength due to significantly suspended sediment concentrations and long ranges [27,30,38]. For the ADVP data (bistatic system), the jump of the *EI* when passing from EXP1 (empty symbols, Figure 9) to EXP2 (full symbols, Figure 9) was presumably a combination of the gain change and increase of backscattering strength (in this case related to bedload concentration change). The dynamic gain change of the UVP (monostatic system) varied only in several instances when changing to more intensive transport conditions. It was then assumed that it contributed to the minor variation between the different repetitions. The difference between the *EI* for 1.5 MHz and 3 MHz for the sandEXP1 (Figure 10b, c) could also be associated with a combination of different gain and eventual shallower samplings of the 3 MHz. The instantaneous dynamic gain might have affected the position of the first peak and the sensitivity to the change of the backscattering strength.

The higher deviation in the *EI* in the UVPs indicated that the monostatic sampling was disturbed by an irregular sediment bed surface, not only in the cells above the maximum value but also in the cells close to the FP, which most probably sampled the immobile surface. The SPro, as a monostatic system, also experienced similar problems in the spatial echo distribution, which may have caused a deviation in the *EI*, especially in the more intense bedload transport conditions [14]. However, the longer pulses and the assumption that the *EI* for the ADCPs is calculated using the trailing edge of the returned pulse [19,26,37] contributed to the consistent influence of the surface scattering, resulting in negligible change when changing from weak to abundant transport conditions (Tables 3 and 4). This was also the case with the UVP cells that fully covered the sediment bed (Figure 10d–f). The latter indicates that the *EI* decreased when both the trailing and leading edge of the pulse fully covered the sediment bed, which might be associated with the sound attenuation into the irregular loose sediment bed [38] and the active bedload layer [26].

These sound losses were also registered by the ADVP. The *EI* decreased for both tested conditions when the profile reached the immobile sediment bed (see passing from circle to triangle symbols in Figure 9). This was evident for both bedload transport conditions but slightly higher when the transport was more abundant; hence, the bed irregularity and sediment concentration were also greater.

5. Conclusions

This study showed that using monostatic and bistatic ultrasound systems in laboratory conditions is a promising technique to measure bedload velocity, one of the most important characteristics of bedload transport. However, both systems showed that inhomogeneous bedload motion introduces

noise and errors in the instantaneous times series, which had to be despiked and time-averaged to obtain reasonable values.

The apparent bedload velocity measured by the bistatic sonar (ADVP) corresponded to the most realistic representation of the true bedload velocity, delivering the full-profile time-averaged velocity of the active layer. This clearly showed that the acoustic geometry plays a crucial role in acoustic sampling, which determines both the backscattering strength from the flume bottom (i.e., *EI*) and the corresponding apparent bedload velocity (v_a).

In general, the bistatic configuration has shown the following advantages:

- A finer cell resolution and the possibility of profiling the bedload velocities.
- The possibility of detecting the thickness of the active bedload layer.
- Easier characterization of the backscattering sources, e.g., the influence of the immobile surface irregularity, isolating the surface from volume scattering.

The ADVP helped to explain some of the assumptions and limitations of the monostatic systems and define the main sources of error in the apparent bedload velocity estimation.

The geometrical components of the monostatic systems, such as the grazing angle, the beam opening, transducer size, together with the internal settings, such as carrying frequency, PRF (velocity range limitation), and pulse length, exhibited a rather complex parameter tuning, which coupled with the nature of bedload mobility and resulted in relatively high deviations in the apparent velocities and echo intensity. For example, the low-carrying frequency transducer (0.5 MHz), in combination with a larger cell size and small transducer resulted, in a five times lower apparent velocity than the true mean bedload velocity and an echo intensity twice less than that measured with higher frequencies transducers (e.g., 1.5 MHz) for the more abundant bedload transport conditions.

This study supported that a careful choice and tuning of monostatic acoustic instrumentation can also lead to more accurate estimation of the bedload velocities and correct backscattering conversion related only to the active bedload layer, which may be useful for field studies where the deployment of ADCP monostatic systems appears to be more feasible than bistatic systems. The following list details the advantages of monostatic acoustic transducers:

- More focused beams, i.e., a smaller beam opening angle, φ, should lead to a more superficial sampling of the bedload. This implied that for a given frequency, a larger transducer should return more realistic data in the absence of water bias.
- A lower frequency (e.g., 0.5 MHz) should be avoided in laboratory conditions because the measured velocities severely underestimated the real bedload velocity. An exception could be considered in cases of high suspended sediments in a water column or a very deep environment where stronger penetration and longer ranges are required [22].
- The finer the resolution, the better the results. This implies shorter pulses for PC but not for the BB, in which the pulse and cell sizes are partially independent [39]. However, in field applications, it is impossible to have a cell size in the range of the bedload active layer. Thus, more attention should be paid to more efficient acoustic sampling.
- The higher grazing angle, θ, results in a higher underestimation of the bedload velocity and less sensitivity in the echo intensity when the bedload transport conditions change. However, it should not be larger than the critical angle of reflection [38].
- The echo intensity might be used as an indicator for the bedload concentration if the cell resolution and source intensity are known a priori.

Echo intensity variations within the bedload profiling (for the bistatic instrument) and for the changing bedload rate were clearly related to the prevailing effect of surface and volume scattering from loose-steady and moving particles, respectively. These two sources of scattering may also correspond to fixed-bottom and water biases [17], respectively, which additionally contribute to an incorrect estimation of the bedload velocity. This evidence indicates that the backscatter measurement from the

riverbed is a good candidate for assessing the reliability of apparent velocity for bedload transport quantification. Therefore, both the apparent velocity and corresponding backscattering strength may be implemented to repair bedload conditions in the field by using ADCPs. This will also require comprehensive backscatter correction due to sound propagation into the water column.

Although a general conclusion is that the bistatic instruments have better acoustic sampling and offer more detailed results, their application is still limited in laboratory conditions (e.g., a maximum range of 400 mm). Future research should be focused on developing a bistatic instrument for field application. Moreover, the existing bistatic sonar should be tested in laboratory conditions with different bedload materials and larger resolutions (i.e., closer to a feasible setting for field use) to examine the sensitivity in those cases.

Regarding the monostatic configuration, more experiments should be conducted to better define the correlation between the transducer characteristics and the measurements of the apparent bedload velocity. The internal signal processing should be focused on the development of finer resolution (e.g., upgrade of the coded element BB modulation) because the bedload active layer in most of the cases has a negligible thickness when compared to the water depth. Finally, multiparameter optimization should be performed to design the best possible configuration for taking bedload measurements.

Author Contributions: Conceptualization, S.C. and M.G.; methodology, S.C., M.G., and R.A.; software, S.C. and M.G.; validation, M.G. and N.R.; formal analysis, S.C. and M.G.; investigation, S.C., M.G. and R.A.; resources, M.G. and N.R.; data curation, S.C., M.G., and R.A.; writing—original draft preparation, S.C.; writing—review and editing, M.G., N.R., and R.A.; visualization, S.C.; supervision, M.G., N.R.; project administration, M.G. and N.R.; funding acquisition, N.R. All authors have read and agreed to the published version of the manuscript.

Funding: This research and the laboratory campaign at NTNU were funded by the Norwegian Research Council and Statkraft as part of the multidisciplinary project SEDIPASS. The laboratory campaign at UniBo was conducted within the preparation phase of the 4th Edition of the W.A.T.E.R. Summer School (Workshop on Advanced measurement Techniques and Experimental Research) supported by the Experimental Methods and Instrumentation Committee of the International Association for Hydro-Environment Engineering and Research IAHR. Both laboratory campaigns were supported by Ubertone, which made available the UB-Lab (UVP) and the UB-Lab 2C (ADVP).

Acknowledgments: The author would like to acknowledge the technical and advisory assistance by Ubertone. Ubertone lent the ADVP and the UVPs and contributed to this study by adjusting the instrument parameters.

Conflicts of Interest: The authors declare no conflict of interest.

References

1. Church, M.; Haschenburger, J.K. What is the "active layer"? *Water Resour. Res.* **2017**, *53*, 5–10. [CrossRef]
2. Hubbell, D.W. *Apparatus and Techniques for Measuring Bedload*; U.S. Government Printing Office: Washington, DC, USA, 1964.
3. Frings, R.M.; Vollmer, S. Guidelines for sampling bedload transport with minimum uncertainty. *Sedimentology* **2017**, *64*, 1630–1645. [CrossRef]
4. Gomez, B. Bedload transport. *Earth Sci. Rev.* **1991**, *31*, 89–132. [CrossRef]
5. Gaweesh, M.; Van Rijn, L. Bed-Load Sampling in Sand-Bed Rivers. *J. Hydraul. Eng.* **1994**, *120*, 12. [CrossRef]
6. Nino, Y.; Garcia, M. Gravel saltation. *Water Resour. Res.* **1994**, *30*, 1915–1919. [CrossRef]
7. Drake, T.G.; Shreve, R.L.; Dietrich, W.E.; Whiting, P.J.; Leopold, L.B. Bedload transport of fine gravel observed by motion-picture photography. *J. Fluid Mech.* **1988**, *192*, 193–217. [CrossRef]
8. Lee, H.; Hsu, I. Investigation of Saltating Particle Motions. *J. Hydraul. Eng.* **1994**, *120*, 831–845. [CrossRef]
9. Lajeunesse, E.; Malverti, L.; Charru, F. Bed load transport in turbulent flow at the grain scale: Experiments and modeling. *J. Geophys. Res. Space Phys.* **2010**, *115*. [CrossRef]
10. Papanicolaou, A.N.; Diplas, P.; Balakrishnan, M.; Dancey, C.L. Computer Vision Technique for Tracking Bed Load Movement. *J. Comput. Civ. Eng.* **1999**, *13*, 71–79. [CrossRef]
11. Keshavarzy, A.; Ball, J. An application of image processing in the study of sediment motion. *J. Hydraul. Res.* **1999**, *37*, 559–576. [CrossRef]
12. Radice, A.; Malavasi, S.; Ballio, F. Solid transport measurements through image processing. *Exp. Fluids* **2006**, *41*, 721–734. [CrossRef]

13. Blanckaert, K.; Heyman, J.; Rennie, C.D. Measuring Bedload Sediment Transport with an Acoustic Doppler Velocity Profiler. *J. Hydraul. Eng.* **2017**, *143*, 04017008. [CrossRef]
14. Conevski, S.; Guerrero, M.; Ruther, N.; Rennie, C. Laboratory investigation of the apparent bedload velocity measured by ADCPs. *J. Hydraul. Eng.* **2019**, *145*, 04019036-17. [CrossRef]
15. Rickenmann, D.; Turowski, J.M.; Fritschi, B.; Klaiber, A.; Ludwig, A. Bedload transport measurements at the Erlenbach stream with geophones and automated basket samplers. *Earth Surf. Process. Landforms* **2012**, *37*, 1000–1011. [CrossRef]
16. Geay, T.; Belleudy, P.; Gervaise, C.; Habersack, H.; Aigner, J.; Kreisler, A.; Seitz, H.; Laronne, J.B. Passive acoustic monitoring of bed load discharge in a large gravel bed river. *J. Geophys. Res. Earth Surf.* **2017**, *122*, 528–545. [CrossRef]
17. Rennie, C.D.; Millar, R.G.; Church, M. Measurement of Bed Load Velocity using an Acoustic Doppler Current Profiler. *J. Hydraul. Eng.* **2002**, *128*, 473–483. [CrossRef]
18. Rennie, C.D. Site specificity of bed load measurement using an acoustic Doppler current profiler. *J. Geophys. Res. Space Phys.* **2004**, *109*. [CrossRef]
19. Rennie, C.D.; Vericat, D.; Williams, R.D.; Brasington, J.; Hicks, M. Calibration of Acoustic Doppler Current Profiler Apparent Bedload Velocity to Bedload Transport Rate. In *Gravel-Bed Rivers: Process and Disasters*; Wiley-Blackwell: Hoboken, NJ, USA, 2017; pp. 209–233.
20. Rennie, C.D.; Church, M. Mapping spatial distributions and uncertainty of water and sediment flux in a large gravel bed river reach using an acoustic Doppler current profiler. *J. Geophys. Res. Space Phys.* **2010**, *115*. [CrossRef]
21. Jamieson, E.C.; Rennie, C.D.; Ramooz, R. Validation of aDcp bedload transport measurements. In Proceedings of the International Conference on Fluvial Hydraulics, Izmir, Turkey, 3–5 September 2008.
22. Gaeuman, D.; Jacobson, R.B. Acoustic bed velocity and bed load dynamics in a large sand bed river. *J. Geophys. Res. Space Phys.* **2006**, *111*. [CrossRef]
23. Ramooz, R.; Rennie, C.D. *Laboratory Measurement of Bedload with an ADCP*; Reston: Virginia, CA, USA, 2008.
24. Latosinski, F.G.; Szupiany, R.N.; Guerrero, M.; Amsler, M.L.; Vionnet, C. The ADCP's bottom track capability for bedload prediction: Evidence on method reliability from sandy river applications. *Flow Meas. Instrum.* **2017**, *54*, 124–135. [CrossRef]
25. Conevski, S.; Guerrero, M.; Rennie, C.D.; Rüther, N. Acoustic sampling effects on bedload quantification using acoustic Doppler current profilers. *J. Hydraul. Res.* **2020**, 1–19. [CrossRef]
26. Conevski, S.; Guerrero, M.; Rennie, C.D.; Ruther, N. Towards an evaluation of bedload transport characteristics by using doppler and backscatter outputs from ADCPs. *J. Hydraul. Res.* **2020**, in press.
27. UBERTONE. *ADVP Measurement Principle—User Manual*; UBERTONE: Schiltigheim, France, 2019.
28. Hurther, D.; Thorne, P.D. Suspension and near-bed load sediment transport processes above a migrating, sand-rippled bed under shoaling waves. *J. Geophys. Res. Oceans* **2011**, *116*. [CrossRef]
29. RDInstruments. StreamPro ADCP Guide. 2015. Available online: https://www.trs-rentelco.com/Specs-Manuals/TELDYN_STREAMPRO_Manual.pdf (accessed on 30 October 2020).
30. UBERTONE. *UB-Lab Acoustic Profiler*; UBERTONE: Schiltigheim, France, 2017.
31. Fernandez-Luque, B.; Van Beek, R. Erosion And Transport Of Bed-Load Sediment. *J. Hydraul. Res.* **1976**, *14*, 127–144. [CrossRef]
32. Abbot, J.; Francis, J. Saltation and suspension trajectories of solid grains in a water stream. *Philos. Trans. R. Soc.* **1977**, *A*, 225–254.
33. Van Rijn, L. Sediment transport, part i: Bed load transport. *J. Hydraul. Eng.* **1984**, *110*, 1431–1456. [CrossRef]
34. Thorne, P.D.; Hanes, D. A review of the acoustic measurement of small-scale sediment processes. *Cont. Shelf Res.* **2002**, 603–632. [CrossRef]
35. Thorne, P.D.; Meral, R. Formulations for the scattering properties of suspended sandy sediments for use in the application of acoustics to sediment transport processes. *Cont. Shelf Res.* **2008**, *28*, 309–317. [CrossRef]
36. Clay, C.S.; Medwin, H. *Fundamentals of Acoustical Oceanography*; Academic Press: Boston, MA, USA; San Diego, CA, USA; New York, NY, USA, 1998.
37. RDInstruments. Acoustic Doppler Current Profiler Principles of Operation a Practical Primer. 2011. Available online: https://www.comm-tec.com/Docs/Manuali/RDI/BBPRIME.pdf (accessed on 30 October 2020).
38. Urick, R.J. *Principles of Underwater Sound*; Peninsula Publishing: Newport Beach, CA, USA, 1983.

39. Brumley, B.H.; Cabrera, R.G.; Deines, K.L.; Terray, E.A. Performance of a broad-band acoustic Doppler current profiler. *IEEE J. Ocean. Eng.* **1991**, *16*, 402–407. [CrossRef]
40. Ivakin, A.N. Underwater sound scattering by volume inhomogeneities of a bottom medium bounded by a rough surface. *Soviet Phys. Acoust.* **1981**, *27*, 2012–2017.